Effect of Ammonium Chloride Electrolyte on the Performance of Graphene Nano Sheets Electrode

Kerista Tarigan *, Rikson Siburian *, Nuni Widiarti, Lisnawaty Simatupang, Yosia Gopas Oetama Manik, Joys Alisa Angelina Hutapea, Jingfeng Huang, Alfred Iing Yoong Tok

Posted Date: 4 June 2026

doi: 10.20944/preprints202606.0364.v1

Keywords: graphene nanosheets; candlenut shell; biomass-derived graphene; ammonium chloride; NH4Cl electrolyte; graphene-based electrode

 doi:10.20944/preprints202606.0364.v1

Article

Effect of Ammonium Chloride Electrolyte on the Performance of Graphene Nano Sheets Electrode

Kerista Tarigan [1,2,*], Rikson Siburian [2,3,4,*], Nuni Widiarti [5], Lisnawaty Simatupang [6], Yosia Gopas Oetama Manik [3,4], Joys Alisa Angelina Hutapea [3,4], Jingfeng Huang [7] and Alfred Iing Yoong Tok [7]

[1] Department of Physics, Faculty of Mathematics and Natural Sciences, Universitas Sumatera Utara, Medan 20155, Indonesia
[2] Carbon and Frankincense Research Center, Universitas Sumatera Utara, Medan 20155, Indonesia
[3] Department of Chemistry, Faculty of Mathematics and Natural Sciences, Universitas Sumatera Utara, Medan 20155, Indonesia
[4] Department of Postgraduate of Chemistry, Faculty of Mathematics and Natural Sciences, Universitas Sumatera Utara, Medan 20155, Indonesia
[5] Chemistry Department, Faculty of Mathematics and Natural Sciences, Universitas Negeri Semarang, Semarang 50229, Indonesia
[6] Department of Chemistry, Faculty of Mathematics and Natural Sciences, Universitas Negeri Medan, Medan 20221, Indonesia
[7] School of Materials Science and Engineering, Nanyang Technological University, 50 Nanyang Avenue, Singapore 639798, Singapore
* Correspondence: kerista@usu.ac.id (K.T.); rikson@usu.ac.id (R.S.)

Abstract

Research on the effect of ammonium chloride (NH_4Cl) electrolyte on graphene nanosheet (GNS) electrodes derived from candlenut shells (Aleurites moluccana (L.) Willd) as primary battery cathodes has been conducted. GNS was synthesized via pyrolysis and modified with NH_4Cl to produce G–N 0.5 M, G–N 1.0 M, G–N 2.0 M, and G–N 3.0 M samples. The materials were characterized using XRD, SEM-EDX, and electrical measurements at 0.5–1.5 V. XRD results show peaks at $2\theta \approx 25°$ and 44.27° corresponding to C(002) and C(100) planes, while G–N samples exhibit new diffraction peaks at (111), (200), (220), (311), (222), and (400), indicating NH_4Cl incorporation. SEM analysis reveals a transition from layered GNS morphology to more wrinkled and agglomerated structures with increasing NH_4Cl concentration, supported by EDX showing decreasing carbon content and the presence of chlorine (up to ~5.9%). Electrical conductivity increases significantly from commercial battery to GNS and further to G–N samples, reaching ~1.30 $S \cdot cm^{-1}$ for G–N 2.0 M, along with energy density (~605 $Wh \cdot kg^{-1}$) and power density (~605 $W \cdot kg^{-1}$). These results indicate that NH_4Cl modification enhances electrochemical performance and highlights the importance of electrolyte variation in optimizing GNS-based electrodes for primary battery applications.

Keywords: graphene nanosheets; candlenut shell; biomass-derived graphene; ammonium chloride; NH_4Cl electrolyte; graphene-based electrode

1. Introduction

Batteries are electrochemical devices that store electrical energy in chemical form, which can later be converted back into electrical energy to generate an electric current. In daily life, two main types of batteries are commonly used: primary batteries and secondary batteries. A primary battery typically consists of three essential components: a carbon rod as the cathode (positive terminal), zinc (Zn) as the anode (negative terminal), and a paste electrolyte [1,2]. The main drawbacks of primary batteries include their limited lifespan and low electrical conductivity. One approach to address these

 doi:10.20944/preprints202606.0364.v1

issues involves the use of graphitic carbon-based materials (C-π), such as graphene, in combination with suitable electrolytes to enhance the efficiency of the electrochemical system [3–5].

Graphene is a two-dimensional carbon material with an sp^2 hybridized structure, forming a flat hexagonal lattice. It possesses exceptional electrical and thermal conductivity [6]. Due to its outstanding properties—such as catalytic activity [7], ultrathin structure (0.335 nm thickness), mechanical strength due to van der Waals bonding, and a high specific surface area of approximately 2630 m^2/g—graphene is widely explored for applications in battery electrodes, supercapacitors, and sensors [8–10]. These advantages make graphene a primary target for large-scale production [11–13]. However, large-scale production of graphene remains challenging due to limitations in raw material availability and insufficient understanding of optimal production techniques. Most existing production methods rely on graphite as the primary raw material. Several studies have proposed that biomass-derived precursors containing cellulose compounds, such as coconut shell [14–16], candlenut (Aleurites moluccana) shells [17,18], corn waste [19], and dead leaf biomass [20]. They can be converted into graphene via pyrolysis, producing the large scale of graphene.

On the other hand, electrolytes play a vital role in ensuring the stability and performance of electrodes in battery systems. Electrolytes are substances that can conduct electric current and are classified into two categories: liquid and solid electrolytes [21–24]. Liquid electrolytes such as ammonium chloride (NH_4Cl) offer several advantages, including low cost, high ionic conductivity, low toxicity, and enhanced safety [25–27]. The electrochemical behavior of zinc electrodes in aqueous NH_4Cl solutions of various concentrations without additives, focusing on their protective effects were investigated [28]. The others research revealed that the concentration of Cl^- and NH_4^+ ions significantly influences the electrochemical behavior of zinc electrodes and highlighted the importance of optimizing NH_4Cl concentration to support efficient ion transport; excessively high concentrations may reduce ion mobility due to increased solution viscosity, whereas lower concentrations allow freer ion movement, thereby increasing conductivity. Interestingly, a concentration of approximately 1 M NH_4Cl in graphene-based systems resulted in optimal electrochemical performance, with pore structures that facilitate faster and more efficient ion transport [29].

In response to the growing demand for environmentally friendly energy solutions, the utilization of biomass-derived graphene, such as that from candlenut shells, represents a promising and sustainable strategy. Siburian reported that graphene synthesized from candlenut shells through pyrolysis at 600 °C demonstrated a current density of up to 1016 A/cm^2. However, previous combinations of Graphene Nano Sheets (GNS) and electrolyte exhibited limitations in homogeneity, which hindered the effectiveness of electrical conductivity testing [30]. Based on these issues, the present study aims to improve the homogeneity of GNS and electrolyte mixtures by processing them into paste form. Therefore, this research investigates the effect of NH_4Cl electrolyte on the performance of GNS electrodes derived from candlenut shells (Aleurites moluccana (L.) Willd) as cathodes in primary batteries. It is expected that this study will contribute to the development of graphene as a superior material for primary batteries and supercapacitor applications. Finally, this research may be expected to analyze the effect of ammonium chloride (NH_4Cl) electrolyte concentration on GNS-based electrodes used as cathodes in primary batteries and to evaluate the electrical conductivity, power density, and energy density of the NH_4Cl/GBN system at various NH_4Cl electrolyte concentrations in paste form.

2. Materials and Methods

2.1. Production of Candlenut Shell Charcoal

First, we produced the charcoal from candlenut shell as a raw material. One kilogram of cleaned candlenut shells was sun-dried and oven-dried at 105 °C for 24 hours. The dried biomass was carbonized at 600 °C for 4 hours to yield charcoal chips.

 doi:10.20944/preprints202606.0364.v1

2.2. Synthesis of Graphene Nano Sheets (GNS)

Charcoal was brushed to remove ash, mixed with activated carbon (1 : 1 weight ratio), and pyrolyzed at 700 °C for 1 hour. The resulting GNS was washed, dried, ground, and sieved [31]. Approximately 680 grams of GNS were obtained.

2.3. Preparation of NH_4Cl Electrolyte Solutions

Each of 0.2675, 0.535, 1.07, and 1.605 g NH_4Cl dissolved in 10 mL water to produce the series of concentrations was labeled as 0.5, 1.0, 2.0, and 3.0 M NH_4Cl solutions, respectively.

2.4. Preparation of Active Materials

For each concentration, 0.3 g of GNS was mixed with 10 mL NH_4Cl solution, stirred for 2 hours, filtered, and dried at 105 °C for 2 hours. This process yielded G-N x (x= 0.5 M, 1.0 M, 2.0 M, and 3M). active powders.

2.5. Characterization

2.5.1. X-Ray Diffraction (XRD)

X-ray diffraction (XRD) analysis was carried out using a Cu Kα radiation source (λ = 1.5406 Å) operated at 40 kV with a monochromator system (Rigaku Corporation, Japan). The measurements were performed using a beam size of 10 mm × 10 mm. The diffraction patterns were recorded over a 2θ range of 20°–90° with a scanning step of 2.0°.

2.5.2. Scanning Electron Microscopy with an Energy-Dispersive X-Ray Spectroscopy (SEM-EDX)

The morphology and microstructure of the samples were examined using SEM-EDX system (JEOL JSM-7600F, Japan). The EDX measurements were conducted at an accelerating voltage of 20 kV, while SEM imaging was performed at 5 kV.

2.5.3. Electrical Conductivity Testing

Electrical conductivity analysis was carried out for each sample using a fuse tube (length = 2.3 cm; diameter = 0.3 cm) filled with the prepared material (mass = 0.15 g). The measurement system consisted of a DC power supply (CODY 3005DT) connected to a digital multimeter (ZOTEK ZT98) to record the electrical response of the samples, following previously reported procedures [3]. The applied voltages were set at 0.5 V, 1.0 V, and 1.5 V, and the resulting current was recorded at different time intervals.

The electrical conductivity (σ) was determined based on the relationship between current, voltage, and the geometric dimensions of the sample. The conductivity can be expressed as:

$$\sigma = \frac{I \times l}{V \times A} \quad (1)$$

where σ is the electrical conductivity ($S \cdot cm^{-1}$), I is the measured current (A), V is the applied voltage (V), L is the length of the sample (cm), and A is the cross-sectional area of the tube (cm^2). This equation is derived from the fundamental relationship between resistance and resistivity, where conductivity is the inverse of resistivity [32].

In addition to conductivity, the electrochemical performance of the samples was evaluated in terms of energy density and power density. The energy density (ED) represents the amount of energy stored per unit mass and was calculated using:

$$ED = \frac{V \times I \times t}{m} \quad (2)$$

where V is the applied voltage (V), I is the current (A), t is the discharge time (hour), and m is the mass of the active material (kg) [33].

 doi:10.20944/preprints202606.0364.v1

Meanwhile, the power density (PD), which indicates the rate at which energy can be delivered, was calculated using:

$$PD = \frac{V \times I}{m} \quad (3)$$

where V is the applied voltage (V), I is the current (A), and m is the mass of the active material (kg) [34].

2.6. Bibliometric Analysis

A bibliometric analysis was conducted to evaluate the research landscape of graphene-based electrochemical systems using data retrieved from the Scopus database. The search query TITLE-ABS-KEY (graphene AND electrode AND electrolyte AND "electrochemical performance") was applied, limited to publications from 2020 to 2025, yielding 962 documents. The data were exported in CSV format and analyzed using VOSviewer software through a keyword co-occurrence approach. A minimum occurrence threshold of 30 was applied to identify relevant keywords, followed by manual refinement to remove irrelevant and duplicate terms, resulting in 55 representative keywords grouped into clusters. Network and overlay visualizations were generated to examine keyword relationships and temporal research trends, while additional analyses, including publication trends, document types, and geographical distribution, were performed using Scopus analytical tools.

3. Results and Discussion

We first evaluate the research trend of graphene for electrochemical applications from 2020 to 2025 to establish a comprehensive understanding of the current scientific landscape. A bibliometric analysis was conducted based on 962 publications retrieved from the Scopus database, followed by keyword co-occurrence mapping using VOSviewer. By applying a minimum occurrence threshold of 30 and subsequent manual refinement, a total of 55 representative keywords were selected and classified into five distinct clusters. The data show that the number of publications increased significantly in 2025, reaching 188 documents, with research articles representing the dominant contribution. In addition, China and India are identified as the leading countries in terms of publication output (Figure 1(a–c)).

The resulting network visualization (Figure 1 (d)) reveals that "graphene", "electrochemical electrodes", and "electrolytes" are the most dominant and highly interconnected keywords, indicating their central role in the research field. The strong linkage among these keywords highlights that current studies are primarily directed toward optimizing the interaction between electrode materials and electrolyte systems to achieve enhanced electrochemical performance.

A more detailed examination of the clustering structure provides insight into the main research directions. The first cluster is associated with electrochemical performance optimization, including keywords such as "electrochemical electrodes", "electrochemistry", and "performance", reflecting efforts to improve efficiency and stability. The second cluster focuses on graphene-based materials and their applications, including "graphene", "supercapacitor", and "electrolytes", emphasizing the dominant role of graphene in energy storage systems. The third cluster relates to material synthesis and structural characteristics, such as "reduced graphene oxide", "carbon", and "morphology", indicating continuous advancements in material design and fabrication techniques. The fourth cluster highlights energy storage applications, including "energy storage", "energy density", and "specific capacitance", which are critical parameters for high-performance devices. The fifth cluster represents electrochemical processes and interfacial phenomena, including "charge transfer" and "conductivity", underscoring the importance of ion transport mechanisms in determining overall device performance. The dominance of graphene-related keywords confirms that graphene remains the core material in electrochemical energy storage research. Moreover, the strong interconnection between graphene, electrolytes, and electrochemical performance suggests that recent research

 doi:10.20944/preprints202606.0364.v1

trends are increasingly focused on improving electrode–electrolyte interactions as a key strategy to enhance device efficiency.

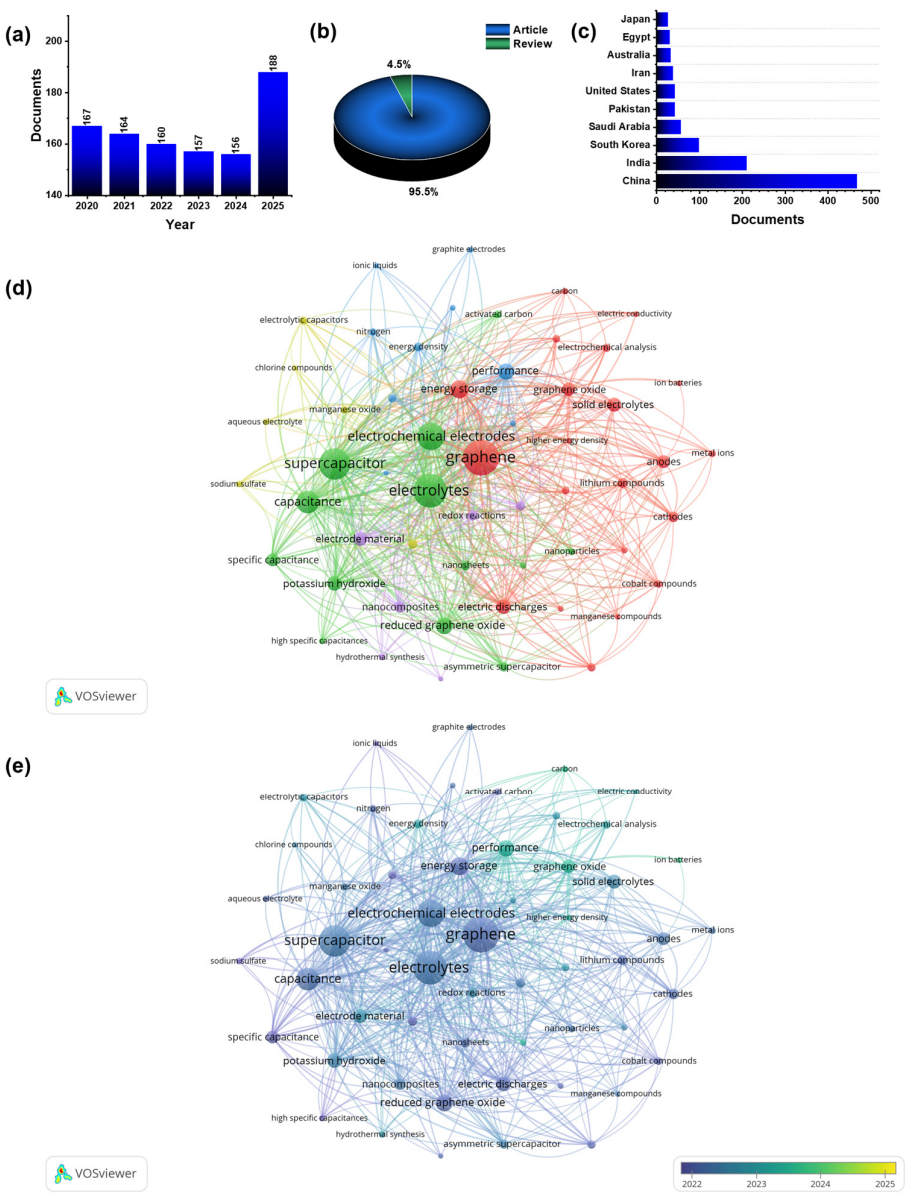

Figure 1. Bibliometric overview of graphene-based electrochemical research (2020–2025). (a) Annual publication trend. (b) Document type distribution. (c) Countries type distribution. (d) Keyword co-occurrence network showing 55 keywords in five clusters. (e) Overlay visualization indicating the temporal evolution of research topics.

The overlay visualization (Figure 1. (e)) further provides insight into the temporal evolution of research topics. Earlier studies were primarily centered on fundamental material properties and conventional electrochemical systems, whereas more recent investigations emphasize advanced graphene-based materials, improved conductivity, and high-performance energy storage applications. Keywords associated with performance optimization and energy-related applications appear more prominently in recent years, indicating a clear transition from fundamental studies toward application-oriented and scalable technologies. This shift suggests that future research will continue to focus on improving electrochemical performance through innovative material design and

 doi:10.20944/preprints202606.0364.v1

advanced electrolyte engineering. In particular, the development of alternative electrolyte systems is expected to play a crucial role in advancing next-generation energy storage technologies.

Notably, keywords related to ammonium chloride (NH_4Cl) are absent from the co-occurrence network, indicating that this electrolyte system has not been widely explored in graphene-based electrochemical research. This absence highlights a significant gap in the current literature. Despite its potential advantages, such as low cost and environmental friendliness, ammonium-based electrolytes remain underutilized. Therefore, the present study focuses on investigating the effect of ammonium chloride electrolyte on the electrochemical performance of graphene nanosheets. To further validate this approach, detailed material characterization and electrochemical analyses, including X-ray diffraction (XRD), scanning electron microscopy coupled with energy-dispersive X-ray spectroscopy (SEM–EDX), and conductivity measurements, are conducted to elucidate the structural, morphological, and electrical properties of the synthesized materials.

3.1. XRD Studies

These findings highlight that structural properties play a crucial role in determining the electrochemical performance of graphene-based materials. Therefore, to further understand the structural characteristics of the synthesized graphene nanosheets, X-ray diffraction (XRD) analysis was performed. The crystalline structure of the synthesized graphene nanosheets was investigated using XRD analysis in order to evaluate the structural ordering and layer stacking of the carbon framework [35]. XRD is a widely used technique for identifying the degree of graphitization and crystallographic arrangement in carbon-based materials, particularly for distinguishing graphitic domains from amorphous carbon structures [36,37]. The diffraction pattern provides important information regarding the interlayer spacing, stacking order, and crystallinity of graphene-derived materials, which are critical parameters influencing their electrochemical performance [38,39].

The XRD diffractogram of GNS derived from candlenut shells displayed characteristic peaks at $2\theta = 25°$ and 44.27°, which correspond to the C (002) and C (100) planes of graphene [40]. These broad and relatively low-intensity peaks are indicative of a predominantly amorphous structure—an expected feature for graphene synthesized from biomass precursors—confirming the successful formation of graphene nanosheets [41,42]. However, the incorporation of NH_4Cl into the G–N samples gradually reduces the intensity of the (002) diffraction peak [43]. This decrease in peak intensity suggests an increase in structural disorder within the graphene layers, which may arise from the interaction of NH_4^+ and Cl^- ions with defect sites and edge regions of the GNS, as presented in Figure 2(a).

Furthermore, the G–N samples exhibit several additional diffraction peaks. For example, the G–N (0.5 M) sample shows peaks at $2\theta = 22.93°$, 32.73°, 40.36°, 46.94°, 52.88°, and 58.40°, corresponding to the (111), (200), (220), (311), (222), and (400) planes of crystalline NH_4Cl, respectively [44,45]. Similar diffraction features are also observed in other G–N samples, although slight shifts in peak positions are detected depending on the NH_4Cl concentration, as shown in Figure 2(b). The presence of these characteristic reflections confirms that NH_4Cl was successfully incorporated into the graphene nanosheet (GNS) matrix.

To further analyze the structural characteristics, peak deconvolution was performed to separate overlapping contributions from crystalline and amorphous phases. This approach enables a more accurate identification of the (002) peak position, which is essential for evaluating structural parameters such as interlayer spacing and crystallinity [46,47,48]. The deconvoluted XRD pattern of pristine GNS is shown in Figure 2(c), where the broad (002) peak can be resolved into multiple components corresponding to amorphous carbon and graphitic domains. The dominant broad feature indicates that the GNS structure is largely disordered with limited graphitic stacking [49,50]. Interestingly, the incorporation of NH_4Cl leads to both a reduction and a shift of the (002) diffraction peak of GNS, indicating structural distortion and strong interaction between the electrolyte and graphene framework. Notably, the (002) peak overlaps with the (111) reflection of crystalline NH_4Cl, complicating peak assignment in the composite system [51]. To address this, a magnified diffraction

 doi:10.20944/preprints202606.0364.v1

region centered on the (111) peak is shown in Figure 2(d), followed by peak deconvolution analysis (Figure 2(e–h)) to resolve the overlapping contributions and provide a more accurate interpretation of the structural evolution [52].

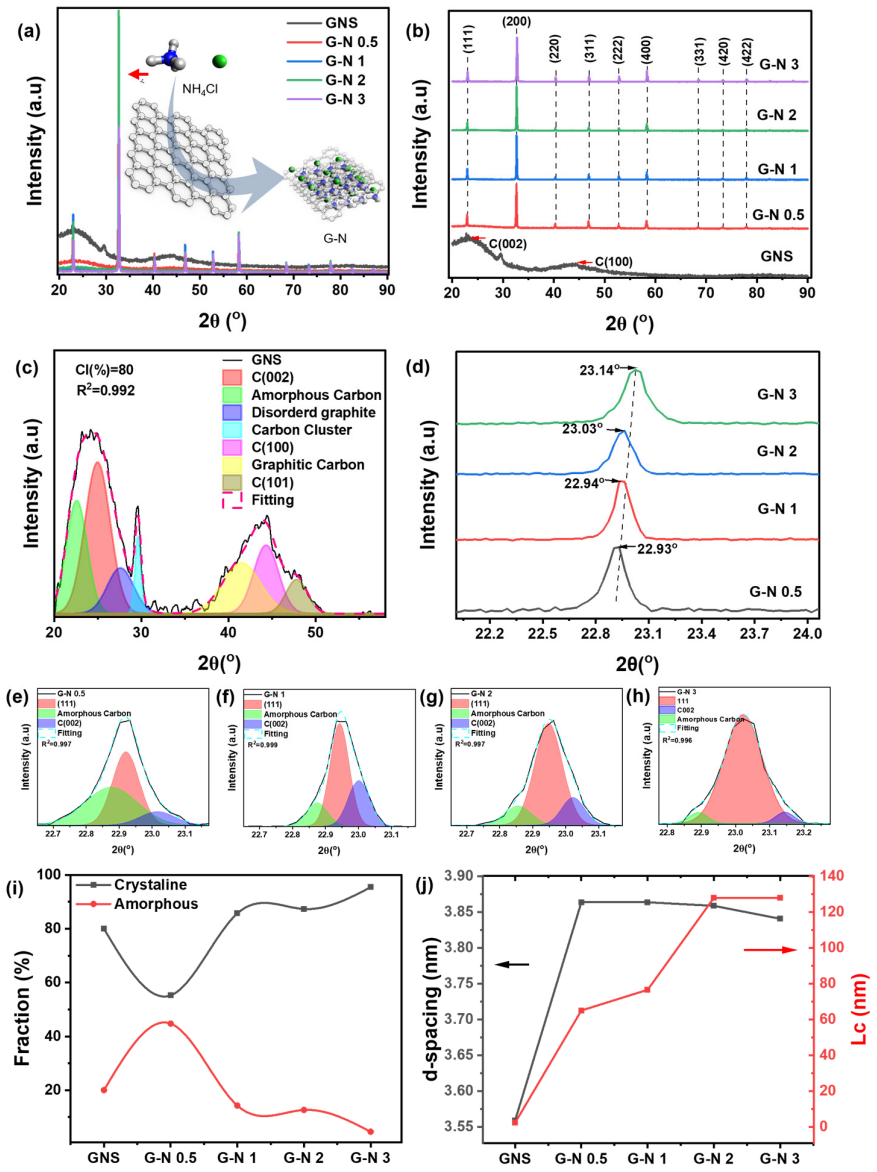

Figure 2. XRD analysis of GNS and NH_4Cl-modified samples (G–N): (a) diffraction patterns and interaction illustration, (b) comparison of patterns, (c) peak deconvolution of GNS, (d) enlarged peaks, (e–h) deconvolution of G–N samples, (i) crystallinity and amorphous fraction, and (j) d-spacing vs crystallite size.

The crystallinity index (CI) was evaluated to quantify the degree of structural ordering in the GNS and G-N samples. The CI reflects the proportion of crystalline regions relative to the overall structure and is commonly used to distinguish between ordered graphitic domains and amorphous carbon phases [53]. A higher CI value indicates a more ordered and graphitic structure, whereas a lower value suggests increased structural disorder [54,55]. The crystallinity index was calculated using the following equation:

$$CI(\%) = \frac{A_c}{A_c + A_A} x100 \quad (4)$$

 doi:10.20944/preprints202606.0364.v1

where A_c is a crystalline area and A_A is an amorphous area. This method enables a reliable comparative evaluation of structural ordering across all samples [56].

The crystallinity index (Figure 2(i)) was evaluated to quantify the degree of structural ordering in the graphene nanosheets after NH_4Cl incorporation. The pristine GNS exhibits a crystallinity of 80%, indicating a moderate level of graphitic ordering with the coexistence of amorphous carbon domains, which is typical for biomass-derived graphene materials [57].

Upon the addition of NH_4Cl at a concentration of 0.5 M, the crystallinity significantly decreases to 55.24%, suggesting a pronounced disruption of the graphene structure. This reduction can be attributed to the initial interaction between NH_4Cl species and the graphene framework, which likely introduces defects, disturbs π–π stacking, and increases the amorphous carbon fraction.

Interestingly, further increasing the NH_4Cl concentration to 1 M and 2 M results in a substantial increase in crystallinity to 85.73% and 86.25%, respectively. This trend indicates a reorganization of the structure, where the presence of NH_4Cl may facilitate partial ordering or contribute to the formation of crystalline domains associated with NH_4Cl phases within the composite system. The coexistence of graphitic and crystalline NH_4Cl phases likely contributes to the overall increase in the calculated crystallinity index. At the highest concentration of 3 M, the crystallinity reaches 95.46%, indicating a highly ordered structure. However, this high value does not necessarily reflect an improvement in graphene ordering alone but is more likely influenced by the dominant contribution of crystalline NH_4Cl phases, as evidenced by the increasing intensity of characteristic diffraction peaks. This suggests that the crystallinity index in composite systems must be interpreted carefully, as it represents the combined contribution of all crystalline phases present. The crystallinity evolution demonstrates a concentration-dependent behavior, where initial NH_4Cl addition induces structural disorder, followed by increased apparent crystallinity due to the growing contribution of crystalline NH_4Cl phases. This finding highlights the dual role of NH_4Cl in modifying both the structural disorder of graphene and the crystalline nature of the composite system, which may significantly influence its electrochemical properties. Therefore, the crystallinity index in this composite system reflects the combined contribution of graphene and NH_4Cl phases rather than the intrinsic ordering of graphene alone [58].

To gain deeper insight into the structural evolution after NH_4Cl impregnation, the diffraction peaks of each sample (GNS, G–N 0.5, G–N 1, G–N 2, and G–N 3) were analyzed quantitatively. The interlayer spacing (d_{002}) of the graphene structure was estimated from the (002) diffraction peak using Bragg's equation:

$$d_{002} = \frac{\lambda}{2 \sin \theta} \quad (5)$$

where λ = 1.5406 Å corresponds to the Cu Kα radiation source [59]. The calculated d_{002} value represents the distance between stacked graphene layers and is widely used to evaluate the degree of graphitic ordering in carbon-based materials [60]. Variations in d_{002} after NH_4Cl incorporation indicate structural distortion and possible expansion of the graphene interlayer spacing, which may arise from the intercalation or interaction of ammonium species within the carbon framework [61].

As shown in Table 1, the variation of crystallinity observed in this study is consistent with the evolution of the interlayer spacing (d_{002}), as presented in Figure 2(j). The pristine GNS exhibits the lowest d_{002} value (3.557 Å), reflecting relatively compact layer stacking with moderate graphitic ordering. Upon NH_4Cl incorporation, a significant increase in d_{002} is observed, reaching a maximum value at G–N (2.0 M) (3.858 Å), followed by G–N (3.0 M) and G–N (1.0 M). This expansion clearly indicates the insertion of NH_4^+ and Cl^- ions into the interlayer region of graphene, which weakens van der Waals interactions and induces layer separation. This expansion further supports the intercalation of ionic species within the graphene layers rather than simple surface adsorption [62,63].

Interestingly, this interlayer expansion correlates with the crystallinity behavior, where an initial decrease at low concentration (0.5 M) is followed by a substantial increase at higher concentrations. The lowest crystallinity at G–N (0.5 M) can be attributed to the initial disruption of graphene stacking without sufficient formation of crystalline NH_4Cl domains. In contrast, at higher concentrations (1–3

 doi:10.20944/preprints202606.0364.v1

M), the increased d_{002} values suggest more effective intercalation, accompanied by the growing contribution of crystalline NH_4Cl phases, which leads to an apparent increase in the overall crystallinity index.

Table 1. Summary of XRD analysis of samples.

Samples	hkl	2θ (°)	FWHM (rad)	d-spacing (Å)	Lc (nm)	CI(%)
GNS	002	25	0.0601	3.558	2.362	80
	100	44.37	0.0590	2.039	2.535	
G-N 0.5	111	22.93	0.0021	3.875	65.014	55.24
G-N 1	111	22.94	0.0018	3.873	76.596	85.73
G-N 2	111	23.03	0.0011	3.858	127.999	86.25
G-N 3	111	23.14	0.0011	3.840	128.024	95.46

The structural ordering of the graphene nanosheets was evaluated through the crystallite size along the c-axis (L_c), which represents the stacking height of graphitic domains [64]. The L_c value was estimated using the Scherrer equation:

$$L_c = \frac{K\lambda}{\beta_{002} \cos \theta_{002}} \quad (6)$$

where L_c is the crystallite size along the c-axis (nm), K is the shape factor (typically 0.89), λ is the X-ray wavelength (commonly 0.15406 nm for Cu Kα radiation), β_{002} is the full width at half maximum (FWHM) of the (002) diffraction peak (in radians), and θ_{002} is the Bragg diffraction angle corresponding to the (002) plane. The Scherrer equation is commonly used to estimate the average crystallite size based on peak broadening in XRD patterns, where narrower peaks indicate larger crystallite domains and improved structural ordering [65].

Further insight into the structural ordering is provided by the crystallite size (L_c), which reflects the stacking height of graphitic domains along the c-axis. The pristine GNS exhibits relatively low L_c values, with 2.362 for the (002) plane and 2.535 for the (100) plane, indicating limited stacking and a predominantly disordered structure. Upon NH_4Cl incorporation, a significant increase in L_c is observed, rising to 65.014 for G–N (0.5 M), 76.596 for G–N (1.0 M), and reaching maximum values of 127.999 and 128.024 for G–N (2.0 M) and G–N (3.0 M), respectively [66].

This substantial increase in L_c suggests the formation of larger coherent crystalline domains within the composite system. However, this increase is likely dominated by the contribution of crystalline NH_4Cl phases rather than intrinsic graphene stacking. However, similar to the crystallinity trend, this increase should not be solely attributed to improved graphene ordering but rather to the growing contribution of crystalline NH_4Cl phases, which dominate the diffraction signal at higher concentrations. The presence of these crystalline domains contributes to an apparent increase in structural ordering, while the graphene framework itself may still experience local disorder and distortion [67].

The highest d_{002} value observed at G–N (2.0 M) suggests that this concentration provides the most effective intercalation of ionic species, resulting in maximum layer expansion and structural distortion [68]. This expanded, and more open structure is expected to enhance ion accessibility and facilitate electrolyte penetration, which is beneficial for electrochemical applications. However, excessive incorporation at higher concentration (3.0 M) may lead to phase domination by NH_4Cl, where the increase in crystallinity and L_c is more influenced by the salt phase rather than intrinsic graphene ordering [69,70].

Overall, these findings demonstrate that NH_4Cl acts as a strong structural modifier, inducing interlayer expansion, increasing defect density, and transforming the graphene nanosheets into a heterogeneous composite system with both disordered carbon and crystalline salt phases [71]. The combined analysis of d_{002}, crystallinity index, and crystallite size (L_c) highlights a concentration-dependent structural evolution governed by intercalation, phase contribution, and structural reorganization.

 doi:10.20944/preprints202606.0364.v1

These structural modifications provide a fundamental basis for understanding the electrochemical behavior discussed in the following sections [72]. To establish a comprehensive structure–property relationship, the structural insights obtained from XRD analysis were further complemented by SEM–EDX characterization to investigate the surface morphology and elemental distribution of the synthesized graphene nanosheets.

3.2. SEM-EDX Studies

SEM-EDX analysis was employed to investigate the surface morphology and elemental composition of GNS and G-N composites. This combined technique provides complementary information on the physical and chemical characteristics of the materials [73,74]. SEM enables detailed observation of surface features such as layer structure, porosity, and aggregation, while EDX provides quantitative analysis of elemental composition [75]. These parameters are essential for understanding the effect of NH_4Cl incorporation on the graphene framework, particularly in relation to electron transport, ion diffusion, and overall electrochemical performance [76].

The morphology of pristine GNS derived from candlenut shells exhibits a typical layered and stacked sheet-like structure with relatively smooth and continuous surfaces, as shown in **Figure 3.** The graphene sheets appear thin, wrinkled, and loosely stacked, forming a porous network with minimal aggregation. This morphology indicates the successful formation of multilayer graphene with a relatively open structure, which is beneficial for providing a large surface area and facilitating ion transport. The well-organized stacking also suggests good structural integrity, which is important for maintaining electrical conductivity [77,78,79].

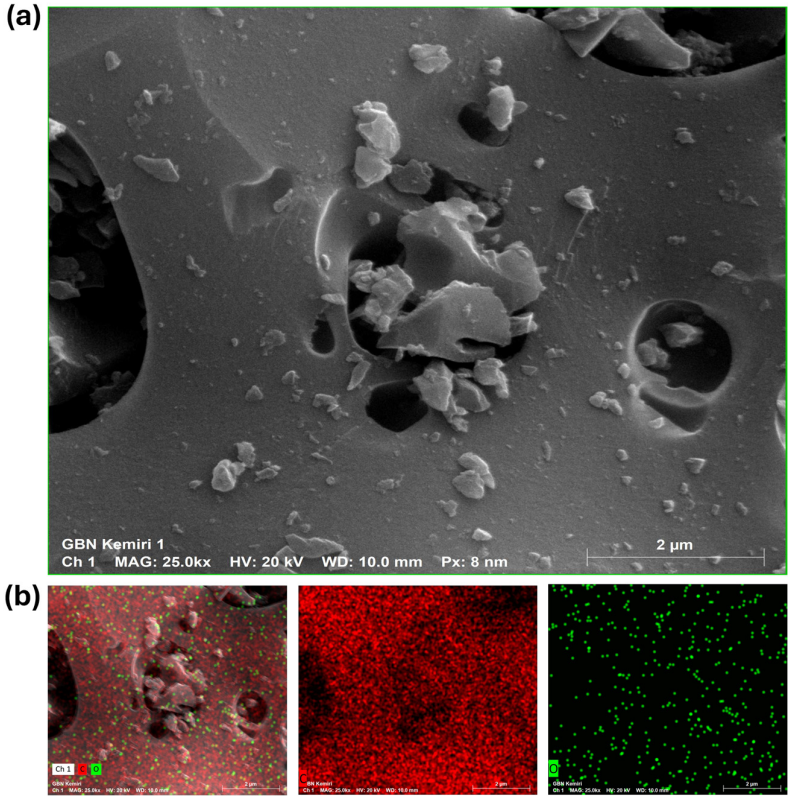

Figure 3. GNS morphology: (a) SEM surface morphology and (b) Corresponding EDX elemental maps for C and O.

The EDX results indicate that GNS is predominantly composed of carbon, with a minor contribution from oxygen. The high carbon content confirms the formation of a graphene-based structure, while the presence of oxygen is associated with residual oxygen-containing functional

 doi:10.20944/preprints202606.0364.v1

groups or slight surface oxidation during the synthesis process [80,81]. These functional groups may originate from the biomass precursor or incomplete carbonization. The absence of other elements indicates that the material has high purity, which is advantageous for maintaining efficient electron transport and minimizing unwanted side reactions [82,83]. We also provide a spectrum of EDX as shown in **Figure S1.**

The incorporation of NH_4Cl induces significant changes in the morphology of the graphene nanosheets. The G–N samples exhibit more irregular, distorted, and partially agglomerated sheet structures compared to pristine GNS, as shown in **Figure 4.** The originally well-defined layered structure becomes less uniform, indicating that the presence of NH_4Cl disrupts the stacking arrangement of graphene layers. This disruption is attributed to the interaction of NH_4^+ and Cl^- ions with the graphene surface, which introduces defects and weakens interlayer interactions [84,85].

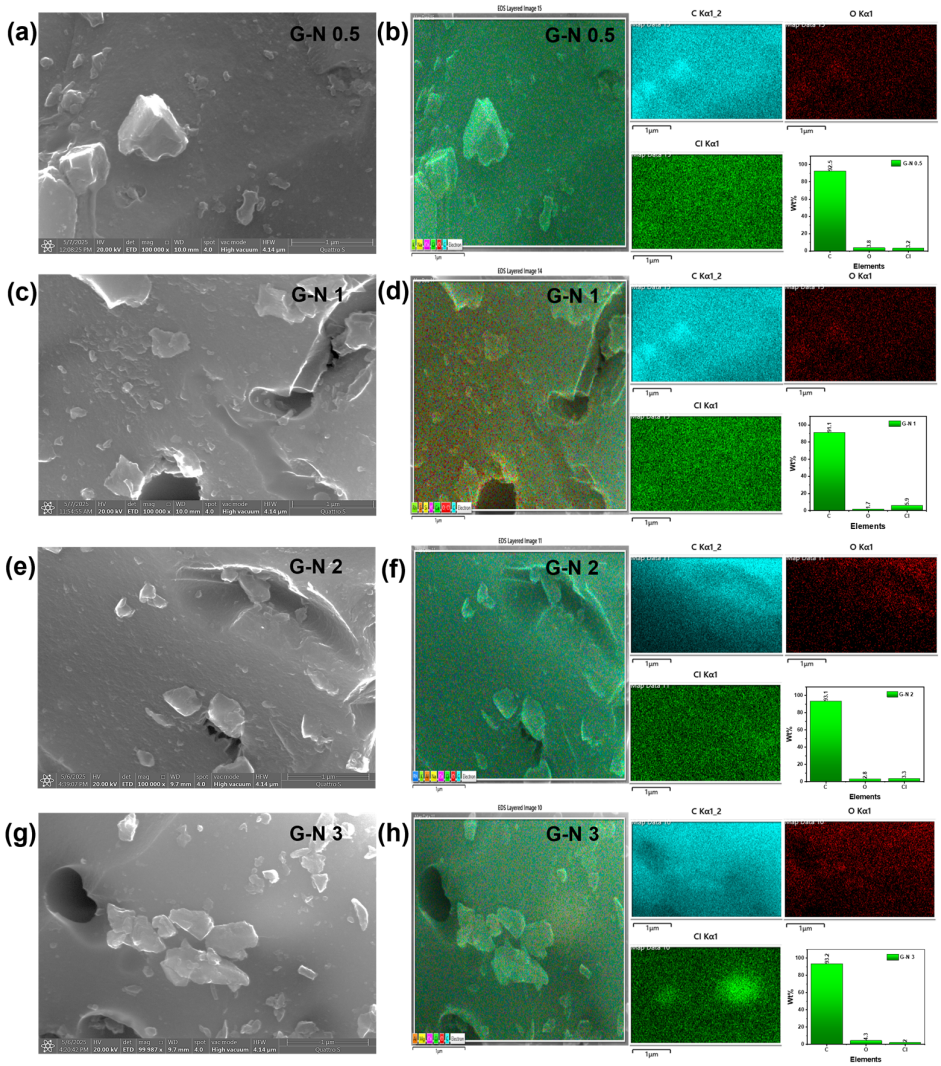

Figure 4. SEM images and EDX elemental mapping of G–N samples at different NH_4Cl concentrations: (a,b) G–N 0.5, (c,d) G–N 1, (e,f) G–N 2, and (g,h) G–N 3. Panels (a,c,e,g) show SEM images, while (b,d,f,h) display the corresponding elemental mapping (C, O, Cl).

As the NH_4Cl concentration increases, the degree of structural modification becomes more pronounced. At lower concentration (0.5 M), the layered morphology is still relatively preserved, although slight roughening and distortion can be observed. At moderate concentration (1.0–2.0 M), the sheets become more wrinkled and disordered, indicating increased defect formation and structural distortion. At higher concentration (3.0 M), the graphene sheets tend to restack and form

 doi:10.20944/preprints202606.0364.v1

denser aggregates, likely due to excessive ionic species promoting particle–particle interaction. These morphological changes result in a more heterogeneous structure, which may enhance ion accessibility but can also reduce structural stability if excessive aggregation occurs [86].

EDX analysis (Table 2) indicates the incorporation of NH_4Cl into the graphene structure, as evidenced by the presence of chlorine in all G–N samples. The carbon content shows a slight decrease compared to pristine GNS, suggesting partial disruption of the carbon framework, while the oxygen content varies with NH_4Cl concentration, reflecting changes in surface functional groups and defect density. Chlorine content increases from 3.2% in G–N 0.5 M to 5.9% in G–N 1.0 M, then decreases at higher concentrations to 3.3% (2.0 M) and 2.0% (3.0 M), likely due to aggregation or saturation effects. This trend indicates that varying NH_4Cl concentrations affect the elemental composition and defect density of graphene, resulting in samples with distinct structural characteristics [87].

In terms of electrode performance, carbon serves as the primary conductive pathway, whereas chlorine provides additional active sites that can enhance ion interaction with the electrolyte. The balance between these elements determines the electrochemical potential of each variation. For instance, G–N (2.0 M) retains a relatively high carbon content (93.1%) while containing sufficient chlorine (3.3%), maintaining conductivity while providing active sites for ion interaction. This composition can be used as a reference to compare the effects of other NH_4Cl concentrations, where lower concentrations may provide fewer active sites and higher concentrations may introduce excessive defects that disrupt conductive pathways [88].

Table 2. Elemental composition of GNS and NH_4Cl-treated samples (G–N series) determined by Energy Dispersive X-ray Spectroscopy (EDX), showing the relative weight percentages (wt%) of detected elements.

Samples	Weight Percentage (wt%)		
	C	O	Cl
GNS	94.67	5.33	-
G-N 0.5	92.5	3.8	3.2
G-N 1	91.1	1.7	5.9
G-N 2	93.1	2.8	3.3
G-N 3	93.2	4.3	2

3.3. Electrical Conductivity Analysis

Electrical conductivity reflects the ability of the electrode material to transport charge efficiently, which is strongly influenced by both electron mobility within the graphene structure and ion transport from the electrolyte [89,90]. In this study, the conductivity behavior demonstrates a clear dependence not only on the applied voltage but also on the electrolyte composition, highlighting the synergistic role of electronic and ionic contributions in the system. Increasing voltage from 0.5 V to 1.5 V consistently enhances conductivity due to the higher driving force for charge movement [91]. Moreover, the introduction of electrolyte species plays a crucial role in facilitating charge transport, as evidenced by the significant improvement in conductivity compared to pristine graphene nanosheets (GNS).

As presented in Figure 5(a–f), a substantial enhancement in electrical conductivity is observed upon NH_4Cl incorporation compared to the pristine GNS. The GNS sample exhibits relatively low conductivity (~0.05–0.09 $S \cdot cm^{-1}$), whereas the addition of NH_4Cl increases conductivity significantly, reaching above 0.5 $S \cdot cm^{-1}$ even at low concentration. The highest conductivity is obtained at 2.0 M NH_4Cl, with values around 1.30–1.31 $S \cdot cm^{-1}$, indicating an optimal ionic environment for charge transport. This enhancement can be attributed to the presence of NH_4^+ and Cl^- ions, which not only improve ionic conductivity but also facilitate the formation of continuous charge transfer pathways within the electrode–electrolyte interface. However, at higher concentration (3.0 M), the conductivity does not increase further and tends to stabilize, suggesting that excessive ionic concentration may lead to ion crowding and increased viscosity, thereby limiting ion mobility. As a result, the system

 doi:10.20944/preprints202606.0364.v1

reaches an optimal condition at 2.0 M, where the balance between ion availability and mobility is maximized [92,93].

The relationship between energy density and power density is illustrated in Figure 5(g–l). A consistent increase in energy density with both applied voltage and electrolyte concentration is observed, indicating enhanced charge storage capability under optimized electrochemical conditions [94,95]. Among all samples, the highest energy density is achieved at 2.0 M NH_4Cl, reaching approximately 605 $Wh{\cdot}kg^{-1}$ at 1.5 V. This significant improvement compared to GNS and the commercial battery can be attributed to enhanced ion diffusion, improved electrical conductivity, and more efficient utilization of active sites within the graphene structure. The incorporation of NH_4Cl enhances the electrochemical activity of graphene by increasing the number of available charge carriers, resulting in better energy storage performance [96].

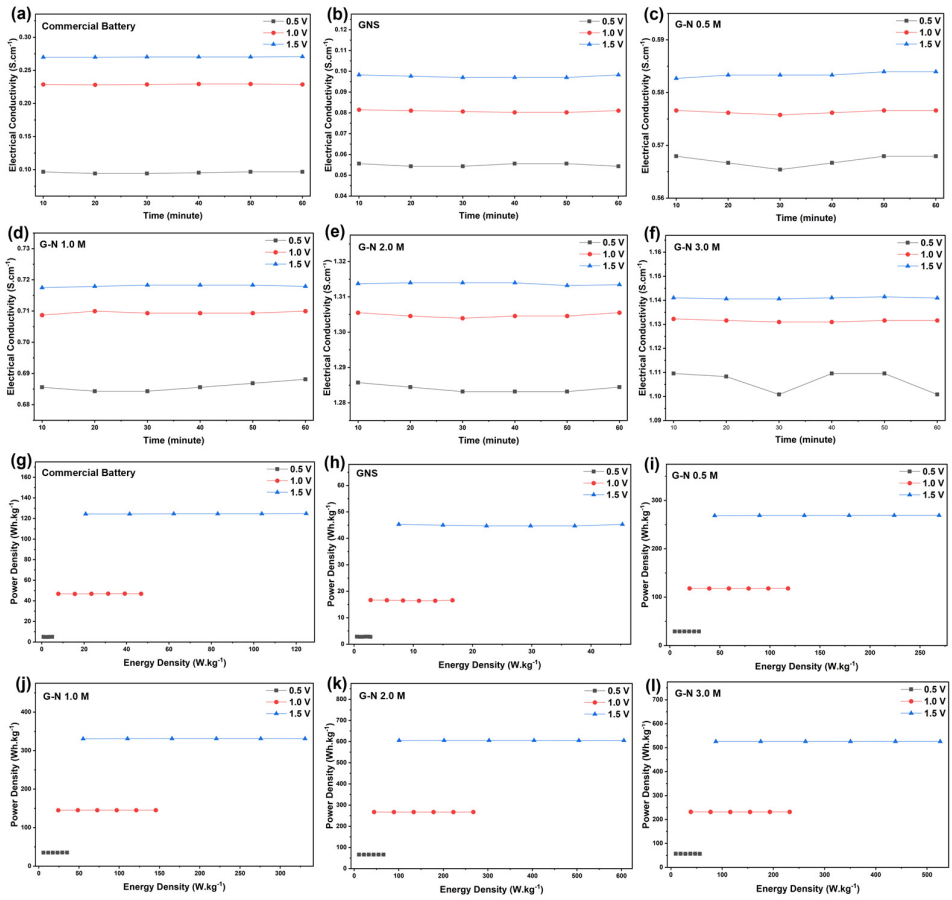

Figure 5. Electrical conductivity (a-f) and relationship between energy density and power density (g–l).

The power density results demonstrate a similar trend, where NH_4Cl-modified electrodes exhibit superior performance compared to GNS and commercial battery. Notably, the optimal performance is again observed at 2.0 M NH_4Cl, where the system achieves a power density of approximately 605 $W{\cdot}kg^{-1}$ at 1.5 V. This indicates that the system is capable of delivering energy rapidly, which is essential for high-performance energy storage devices. The improved power density is closely associated with enhanced electrical conductivity and reduced internal resistance, enabling faster charge–discharge kinetics and more efficient energy delivery [97]. However, at higher concentration (3.0 M), no significant improvement is observed, further confirming that excessive ion concentration can hinder ion mobility and limit overall electrochemical performance. Therefore, 2.0 M NH_4Cl provides the best overall performance, as it offers an optimal balance between ion transport, electrical conductivity, and electrochemical activity, resulting in simultaneously high energy density and power density [98,99,100]. All summary data was tabulated in Table S1.

 doi:10.20944/preprints202606.0364.v1

From an electrode performance perspective, these results clearly demonstrate that NH_4Cl electrolyte plays a dual role in enhancing both charge transport and charge storage mechanisms. The improved electrical conductivity indicates more efficient electron transfer within the graphene network, while the increased energy and power densities reflect enhanced ion diffusion and faster electrochemical kinetics at the electrode–electrolyte interface. This suggests that the electrolyte does not merely act as an ionic medium but actively modifies the electrochemical behavior of the graphene electrode [101,102].

Furthermore, the optimal performance observed at 2.0 M NH_4Cl highlights the importance of electrolyte optimization in achieving high-performance electrodes. At this concentration, the system achieves a balance between ion availability and mobility, enabling efficient ion transport, rapid charge–discharge processes, and effective utilization of active sites. In contrast, excessive electrolyte concentration leads to transport limitations, which negatively affect overall electrode performance.

These findings confirm that the electrochemical performance of graphene nanosheet electrodes is strongly governed by electrolyte-induced modifications, where NH_4Cl enhances conductivity, promotes ion accessibility, and improves charge storage capability. Therefore, controlling electrolyte concentration is a key strategy for optimizing graphene-based electrodes for advanced energy storage applications [29].

4. Conclusions

This study demonstrates that the incorporation of NH_4Cl electrolyte significantly influences the structural, morphological, and electrochemical properties of graphene nanosheets (GNS) derived from candlenut shells. XRD analysis confirms successful NH_4Cl integration, as indicated by the appearance of crystalline peaks, increased interlayer spacing, and reduced crystallinity, reflecting enhanced structural disorder. SEM-EDX results reveal morphological transformation from layered sheets to more distorted structures and confirm the presence of chlorine, indicating effective electrolyte incorporation and its role in modifying the graphene framework.

Electrochemical results show that NH_4Cl concentration plays a key role in determining electrode performance. The G–N (2.0 M) sample exhibits the highest electrical conductivity (~1.30 $S \cdot cm^{-1}$), energy density (~605 $Wh \cdot kg^{-1}$), and power density (~605 $W \cdot kg^{-1}$). This optimal performance is attributed to the balanced interaction between ion availability and mobility, which enhances charge transport and storage. At higher concentration (3.0 M), performance slightly decreases due to ion crowding effects. Overall, G–N (2.0 M) demonstrates strong potential as an efficient and environmentally friendly cathode material for energy storage applications.

Supplementary Materials: The following supporting information can be downloaded at the website of this paper posted on Preprints.org, Figure S1: EDX spectra of GNS, G–N 0.5 M, G–N 1.0 M, G–N 2.0 M, and G–N 3.0 M; Table S1: Summary of conductivity, energy density, and power density of commercial battery, GNS, G–N 0.5 M, G–N 1.0 M, G–N 2.0 M, and G–N 3.0 M.

Author Contributions: Conceptualization, R.S.; methodology, Y.G.O.M.; investigation, K.T. and Y.G.O.M.; data curation, N.W., L.S., J.A.A.H., J.H., and A.I.Y.T.; writing—original draft preparation, K.T. and R.S.; writing—review and editing, R.S., N.W., L.S., Y.G.O.M., J.A.A.H., J.H., and A.I.Y.T.; supervision, R.S.; funding acquisition, J.H.; resources, R.S. All authors have read and agreed to the published version of the manuscript.

Funding: This Research is funded by the Indonesian Endowment Fund for Education (LPDP) on behalf of the Indonesian Ministry of Higher Education, Science, and Technology, and managed under the EQUITY program (Contract No. 095/UN5.1.R/SK/DI.05.03/2025).

Institutional Review Board Statement: Not applicable.

Informed Consent Statement: Not applicable.

Data Availability Statement: The original contributions presented in this study are included in the article/supplementary material. Further inquiries can be directed to the corresponding authors.

 doi:10.20944/preprints202606.0364.v1

Acknowledgments: The authors gratefully acknowledge Petra Melinda Hutagalung, Department of Postgraduate of Chemistry, Faculty of Mathematics and Natural Sciences, Universitas Sumatera Utara, for her valuable assistance.

Conflicts of Interest: The authors declare no conflicts of interest.

References

1. Kichou, S.; Markvart, T.; Wolf, P.; Silvestre, S.; Chouder, A. A Simple and Effective Methodology for Sizing Electrical Energy Storage (EES) Systems Based on Energy Balance. *J. Energy Storage* **2022**, *49*, 104085, doi:10.1016/j.est.2022.104085.
2. Prabhakar, K.; Jain, S.K.; Padhy, P.K. Inertia Estimation in Modern Power System : A Comprehensive Review. *Electr. Power Syst. Res.* **2022**, *211*, 108222, doi:10.1016/j.epsr.2022.108222.
3. Siburian, R.; Paiman, S.; Hutagalung, F.; Ali, A.M.M.; Simatupang, L.; Goei, R.; Rusop, M.M. Facile Method to Synthesize of Magnesium-Graphene Nano Sheets for Candidate of Primary Battery Electrode. *Colloids Interface Sci. Commun.* **2022**, *48*, 100612, doi:10.1016/j.colcom.2022.100612.
4. Siburian, R.; Hutagalung, F.; Silitonga, O.; Paiman, S.; Simatupang, L.; Simanjuntak, C.; Aritonang, S.P.; Alias, Y.; Jing, L.; Goei, R.; et al. The New Materials for Battery Electrode Prototypes. *Materials (Basel).* **2023**, *16*, 555, doi:10.3390/ma16020555.
5. Siburian, R.; Paiman, S.; Hutagalung, F.; Marwan Ali, A.M.; Simatupang, L.; Goei, R.; Rusop, M.M. Developing Nickel/Graphene Nano Sheets as an Alternative Primary Battery Anode. *Ceram. Int.* **2022**, *48*, 12897–12905, doi:10.1016/j.ceramint.2022.01.162.
6. Singh, R.; Rawat, H.; Kumar, A.; Gandhi, Y. Graphene and Its Hybrid Nanocomposite : A Metamorphoses Elevation in the Field of Tissue Engineering. *Heliyon* **2024**, *10*, e33542, doi:10.1016/j.heliyon.2024.e33542.
7. Yadav, P.; Sharma, P.; Roy, T.; Kumar, A.; Kumar, D.; Mudila, H.; Praveen, S.; Ghotekar, S.; Mujawar, N.; Hosseini-bandegharaei, A.; et al. Exploring Catalytic Applications of Graphene-Transition Metal Oxide Nanocomposites for next-Generation Catalysis : A Review. *Inorg. Chem. Commun.* **2025**, *178*, 114506, doi:10.1016/j.inoche.2025.114506.
8. Urade, A.R.; Lahiri, I.; Suresh, K.S. Graphene Properties, Synthesis and Applications: A Review. *Jom* **2023**, *75*, 614–630, doi:10.1007/s11837-022-05505-8.
9. Emon, S.H.; Hossain, M.I.; Khanam, M.; Yi, D.K. Expanding Horizons: Taking Advantage of Graphene's Surface Area for Advanced Applications. *Appl. Sci.* **2025**, *15*, 4145, doi:10.3390/app15084145.
10. Du, Y.; Wang, M.; Ye, X.; Liu, B.; Han, L.; Jafri, S.H.M.; Liu, W.; Zheng, X.; Ning, Y.; Li, H. Advances in the Field of Graphene-Based Composites for Energy–Storage Applications. *Crystals* **2023**, *13*, 912, doi:10.3390/cryst13060912.
11. Ketema, A.; Worku, D. Results in Chemistry Recent Advances of Graphene-Based Materials for Emerging Technologies. *Results Chem.* **2023**, *5*, 100971, doi:10.1016/j.rechem.2023.100971.
12. Ivy, B.; Manisa, V.K.; Lekgoba, T.; Ntuli, F.; Kandjou, V. Coal to Graphene-Based Materials : Evaluating Coal as a Potential Feedstock to Pave Way for Large Scale Production of Graphene and Related Materials , a Review. *Next Mater.* **2025**, *7*, 100519, doi:10.1016/j.nxmate.2025.100519.
13. Wu, Y.; Li, Y.; Zhang, X. The Future of Graphene: Preparation from Biomass Waste and Sports Applications. *Molecules* **2024**, *29*, 1825, doi:10.3390/molecules29081825.
14. Tarigan, K.; Siburian, R.; Anshori, I.; Widiarti, N.; Alias, Y.B.; Goh, B.T.; Huang, J.; Bahfie, F.; Manik, Y.G.O.; Goei, R.; et al. Synthesis and Characterization of Coconut-Derived Graphene Nano Sheet (GNS) and Its Properties in Nickel/GNS and Zinc/GNS Hybrid Electrodes. *Processes* **2024**, *12*, 1943, doi:10.3390/pr12091943.
15. Manik, Y.G.O.; Goh, B.T.; Siburian, R. Low-Cost Synthesis of Biochar-Like Graphene From Coconut Shells: Enhancing Conductivity for Electrochemical Applications. *Rasayan J. Chem.* **2025**, *18*, 318–324, doi:10.31788/RJC.2025.1819132.
16. Siburian, R.; Tang, L.W.; Alias, Y.; Tok, A.I.Y.; Goei, R.; Simanjuntak, C.; Tarigan, K.; Paiman, S.; Goh, B.T.; Anshori, I.; et al. Coconut Waste to Green Nanomaterial: Large Scale Synthesis of N-Doped Graphene Nano Sheets. *Nano-Structures and Nano-Objects* **2023**, *36*, 101061, doi:10.1016/j.nanoso.2023.101061.

 doi:10.20944/preprints202606.0364.v1

17. Tarigan, K.; Siburian, R.; Ching, Y.; Gopas, Y.; Manik, O.; Alisa, J.; Hutapea, A.; Goei, R.; Iing, A.; Tok, Y.; et al. Facile Synthesis of Neodymium-Doped Biomass-Derived Graphene Nanosheets and Electrochemical Properties. *Curr. Res. Green Sustain. Chem.* **2025**, *11*, 100491, doi:10.1016/j.crgsc.2025.100491.
18. Manik, Y.G.O.; Goh, B.T.; Siburian, R.; Alias, Y. Synthesis of Graphene Nanosheets from Coconut and Candlenut Shells: Large-Scale Production and Application in Fe Ion Adsorption and Electrochemical Properties. *ACS Omega* **2025**, *10*, 3338–3350, doi:10.1021/acsomega.4c05745.
19. Tarigan, K.; Siburian, R.; Tang, L.W.; Hutagalung, F.; Pasaribu, L.; Manik, Y.G.O.; Goei, R.; Bahfie, F.; Goh, B.T.; Manawan, M.T.E.; et al. New Route Producing Large-Scale Graphene Nanosheets from Corn Waste for Electrochemical Material New Route Producing Large-Scale Graphene Nanosheets from Corn Waste for Electrochemical Material. *Adv. J. Chem. , Sect. A* **2025**, *8*, 443–445, doi:10.48309/AJCA.2025.466487.1586.
20. Arunpandian, R.; Kumar, M.; Lasalle B, S.I.; Vijayakumar, P.; Chang, J.H. Hierarchical Synthesis of Multi-Layer Graphene-like and Nitrogen-Doped Graphitized Carbon from Dead Leaf Biomass for High-Performance Energy Storage and CO_2 Capture. *J. Taiwan Inst. Chem. Eng.* **2025**, *172*, doi:10.1016/j.jtice.2025.106100.
21. Toprakci, H.A.K.; Toprakci, O. Recent Advances in New-Generation Electrolytes for Sodium-Ion Batteries. *Energies* **2023**, *16*, 3169, doi:doi.org/10.3390/ en16073169 Academic.
22. Liu, Q.; Jiang, W.; Munoz, M.J.P.; Liu, Y.; Yang, Z.; Bloom, I.; Dzwiniel, T.L.; Li, Y.; Pupek, K.Z.; Zhang, Z. Stabilized Electrode/Electrolyte Interphase by a Saturated Ionic Liquid Electrolyte for High-Voltage NMC532/Si-Graphite Cells. *ACS Appl. Mater. Interfaces* **2020**, *12*, 23035–23045, doi:10.1021/acsami.0c06038.
23. Ingole, R.S.; Rajagopal, R.; Mukhan, O.; Kim, S.S.; Ryu, K.S. LiNi0.6Co0.2Mn0.2O2 Cathode-Solid Electrolyte Interfacial Behavior Characterization Using Novel Method Adopting Microcavity Electrode. *Molecules* **2023**, *28*, 3537, doi:10.3390/molecules28083537.
24. Badi, N.; Theodore, A.M.; Alghamdi, S.A.; Al-Aoh, H.A.; Lakhouit, A.; Singh, P.K.; Norrrahim, M.N.F.; Nath, G. The Impact of Polymer Electrolyte Properties on Lithium-Ion Batteries. *Polymers (Basel).* **2022**, *14*, 3101, doi:10.3390/polym14153101.
25. Mauger, A.; Julien, C.M.; Paolella, A.; Armand, M.; Zaghib, K. Building Better Batteries in the Solid State: A Review. *Materials (Basel).* **2019**, *12*, 3892, doi:10.3390/ma122333892.
26. Nestler, T.; Roedern, E.; Uvarov, N.F.; Hanzig, J.; Elia, G.A.; De Vivanco, M. Separators and Electrolytes for Rechargeable Batteries: Fundamentals and Perspectives. *Phys. Sci. Rev.* **2018**, *4*, 1–29, doi:10.1515/psr-2017-0115.
27. Zhu, N.; Zhang, K.; Wu, F.; Bai, Y.; Wu, C. Ionic Liquid-Based Electrolytes for Aluminum/Magnesium/Sodium-Ion Batteries Na. *Energy Mater. Adv.* 2021, *2021*, 614–623.
28. Moulai, F.; Messaoudi, B.; Zerroual, L.; Hadjersi, T.; Manseri, A.; Pireaux, J.J.; Achour, A. Corrosion Attenuation of Zinc Electrode in Zn−MnO2 Battery by Shielding Effect in an Aqueous Ammonium Chloride Electrolyte. *Eur. Phys. J. Plus* **2021**, *136*, 360, doi:10.1140/epjp/s13360-021-01341-y.
29. Wimalasiri, Y.; Mossad, M.; Zou, L. Thermodynamics and Kinetics of Adsorption of Ammonium Ions by Graphene Laminate Electrodes in Capacitive Deionization. *Desalination* **2015**, *357*, 178–188, doi:10.1016/j.desal.2014.11.015.
30. Siburian, R.; Tarigan, K.; Manik, Y.G.O.; Hutagalung, F.; Alias, Y.; Chan, Y.C.; Chang, B.P.; Siow, J.; Ong, A.J.; Huang, J.; et al. Converting Candlenut Shell Waste into Graphene for Electrode Applications. *Processes* **2024**, *12*, 1544, doi:10.3390/pr12081544.
31. Supeno, M.; Siburian, R. New Route: Convertion of Coconut Shell Tobe Graphite and Graphene Nano Sheets. *J. King Saud Univ.—Sci.* **2020**, *32*, 189–190, doi:10.1016/j.jksus.2018.04.016.
32. Saleemi, S.; Aouraghe, M.A.; Wei, X.; Liu, W.; Liu, L.; Siyal, M.I.; Bae, J.; Xu, F. Bio-Inspired Hierarchical Carbon Nanotube Yarn with Ester Bond Cross-Linkages towards High Conductivity for Multifunctional Applications. *Nanomaterials* **2022**, *12*, 208, doi:10.3390/nano12020208.
33. Wannasen, L.; Chanlek, N.; Siriroj, S.; Maensiri, S.; Swatsitang, E.; Pinitsoontorn, S. Enhanced Electrochemical Performance of Sugarcane Bagasse-Derived Activated Carbon via a High-Energy Ball Milling Treatment. *Nanomaterials* **2022**, *12*, 3555, doi:10.3390/nano12203555.

 doi:10.20944/preprints202606.0364.v1

34. Luo, Z.; Wang, X.; Chen, D.; Chang, Q.; Xie, S.; Ma, Z.; Lei, W.; Pan, J.; Pan, Y.; Huang, J. Ultrafast Li/Fluorinated Graphene Primary Batteries with High Energy Density and Power Density. *ACS Appl. Mater. Interfaces* **2021**, *13*, 18809–18820, doi:10.1021/acsami.1c02064.
35. Yin, H.; Gao, X.; Liu, J.; Chen, P. Synthesis of N-Doped Few-Layer Graphene through Shock-Induced Carbon Fixation from CO2. *Nanomaterials* **2023**, *13*, 109, doi:10.3390/nano13010109.
36. Kokmat, P.; Surinlert, P.; Ruammaitree, A. Growth of High-Purity and High-Quality Turbostratic Graphene with Different Interlayer Spacings. *ACS Omega* **2023**, *8*, 4010–4018, doi:10.1021/acsomega.2c06834.
37. Zeng, H.; Xing, B.; Cao, Y.; Xu, B.; Hou, L.; Guo, H.; Cheng, S.; Huang, G.; Zhang, C.; Sun, Q. Insight into the Microstructural Evolution of Anthracite during Carbonization-Graphitization Process from the Perspective of Materialization. *Int. J. Min. Sci. Technol.* **2022**, *32*, 1397–1406, doi:10.1016/j.ijmst.2022.06.009.
38. Salverda, M.; Thiruppathi, A.R.; Pakravan, F.; Wood, P.C.; Chen, A. Electrochemical Exfoliation of Graphite to Graphene-Based Nanomaterials. *Molecules* **2022**, *27*, 8643, doi:10.3390/molecules27248643.
39. Xia, P.; Zhang, Z.; Tang, Z.; Xue, Y.; Li, J.; Yang, G. Preparation and Electrochemical Performance of Three-Dimensional Vertically Aligned Graphene by Unidirectional Freezing Method. *Molecules* **2022**, *27*, 376, doi:10.3390/molecules27020376.
40. Azmi, M.A.; Samosir, F.R.; Syaida, A.A.R.; Jalil, M.T.M.; Jamil, N.M.; Nor, N.H.M.; Siburian, R.; Yahya, M.F.Z.R. Exploring the Antibacterial and Antibiofilm Potential of Graphene Nanosheets Synthesized from Candlenut Shell Waste. *Microb. Pathog.* **2026**, *214*, 108426, doi:10.1016/j.micpath.2026.108426.
41. Supeno, M.; Simanjuntak, C.; Siburian, R. Facile and Benign Method to Produce Large Scale Graphene Nano Sheets. *Iran. J. Chem. Chem. Eng.* **2020**, *39*, 211–214, doi:10.30492/ijcce.2019.36707.
42. Prekodravac, J.R.; Kepić, D.P.; Colmenares, J.C.; Giannakoudakis, D.A.; Jovanović, S.P. A Comprehensive Review on Selected Graphene Synthesis Methods: From Electrochemical Exfoliation through Rapid Thermal Annealing towards Biomass Pyrolysis. *J. Mater. Chem. C* **2021**, *9*, 6722–6748, doi:10.1039/d1tc01316e.
43. Destiarti, L.; Riyanto, R.; Roto, R.; Mudasir, M. Electrolyte Effect in Electrochemical Exfoliation of Graphite. *Mater. Chem. Phys.* **2023**, *302*, 127713, doi:10.1016/j.matchemphys.2023.127713.
44. Pajarito, B.B.; Llorens, C.; Tsuzuki, T. Effects of Ammonium Chloride on the Yield of Carbon Nanofiber Aerogels Derived from Cellulose Nanofibrils. *Cellulose* **2019**, *26*, 7727–7740, doi:10.1007/s10570-019-02645-0.
45. Luo, B.; Yao, Z.; Xiao, X.; Hang, Z.; Jiang, F.; Liu, M.; Chen, L. Hydrogen Desorption from MgH2+NH4Cl/Graphene Composites at Low Temperatures. *Mater. Chem. Phys.* **2021**, *263*, 124342, doi:10.1016/j.matchemphys.2021.124342.
46. Farinre, O.Z.; Alghamdi, H.; Mhatre, S.M.; Kelley, M.L.; Biacchi, A.J.; Davydov, A. V.; Hacker, C.A.; Rigosi, A.F.; Misra, P. Comprehensive Data via Spectroscopy and Molecular Dynamics of Chemically Treated Graphene Nanoplatelets. *Data* **2022**, *7*, 38, doi:10.3390/data7040038.
47. Yao, W.; Weng, Y.; Catchmark, J.M. Improved Cellulose X-Ray Diffraction Analysis Using Fourier Series Modeling. *Cellulose* **2020**, *27*, 5563–5579, doi:10.1007/s10570-020-03177-8.
48. Montoya-Escobar, N.; Ospina-Acero, D.; Velásquez-Cock, J.A.; Gómez-Hoyos, C.; Serpa Guerra, A.; Gañan Rojo, P.F.; Vélez Acosta, L.M.; Escobar, J.P.; Correa-Hincapié, N.; Triana-Chávez, O.; et al. Use of Fourier Series in X-Ray Diffraction (XRD) Analysis and Fourier-Transform Infrared Spectroscopy (FTIR) for Estimation of Crystallinity in Cellulose from Different Sources. *Polymers (Basel).* **2022**, *14*, 5199, doi:10.3390/polym14235199.
49. Li, J.; Qin, Y.; Shen, J.; Chen, Y. Evolution of Carbon Nanostructures during Coal Graphitization : Insights from X-Ray Diffraction and High-Resolution Transmission Electron Microscopy. *Energy* **2024**, *290*, 130316, doi:10.1016/j.energy.2024.130316.
50. Andreoli, S.; Eser, S. Relating Reactivity to Structure in Cokes and Carbon Materials : Temperature-Programmed Oxidation and Microscopy Techniques. *Carbon N. Y.* **2020**, *168*, 362–371, doi:10.1016/j.carbon.2020.06.071.
51. Wang, Y.; Zhu, Y.; Wu, H. Formation and Topological Structure of Three- Dimensional Disordered Graphene Networks †. *Phys. Chem. Chem. Phys.* **2021**, *23*, 10290–10302, doi:10.1039/d1cp00617g.

 doi:10.20944/preprints202606.0364.v1

52. Coelho, A.A. Deconvolution of Instrument and K a 2 Contributions from X-Ray Powder Diffraction Patterns Using Nonlinear Least Squares with Penalties Research Papers. **2018**, 112–123, doi:10.1107/S1600576717017988.
53. Kourtidou, D.; Karfaridis, D.; Kehagias, T.; Vourlias, G.; Bikiaris, D.N.; Chrissafis, K. Incorporating Graphene Nanoplatelets and Carbon Nanotubes in Biobased Poly(Ethylene 2,5-Furandicarboxylate): Fillers' Effect on the Matrix's Structure and Lifetime. *Polymers (Basel).* **2023**, *15*, doi:10.3390/polym15020401.
54. Li, J.; Wang, L.; Cao, D. Investigation on Spectroscopy Characteristics of Different Metamorphic Degrees of Coal-Based Graphite. *Front. Earth Sci.* **2024**, *12*, 1–9, doi:10.3389/feart.2024.1413019.
55. Zhang, Q.; Wei, Q.; Huang, K.; Liu, Z.; Ma, W.; Zhang, Z.; Zhang, Y.; Cheng, H.M.; Ren, W. Defects Boost Graphitization for Highly Conductive Graphene Films. *Natl. Sci. Rev.* **2023**, *10*, 12–15, doi:10.1093/nsr/nwad147.
56. de Oliveira Aguiar, V.; Roget Rodriguez Pita, V.J.; de Fatima Vieira Marques, M.; Soares, I.T.; Martins Ferreira, E.H.; Oliveira, M.S.; Monteiro, S.N. Ultra-High Molecular Weight Polyethylene Nanocomposites Reinforced with Novel Surface Chemically Modified Sonic-Exfoliated Graphene. *J. Mater. Res. Technol.* **2021**, *11*, 1932–1941, doi:10.1016/j.jmrt.2021.02.027.
57. Zhou, Y.; He, J.; Chen, R.; Li, X. Recent Advances in Biomass-Derived Graphene and Carbon Nanotubes. *Mater. Today Sustain.* **2022**, *18*, 100138, doi:10.1016/j.mtsust.2022.100138.
58. Wang, S.; Wang, C.; Ji, X. Towards Understanding the Salt-Intercalation Exfoliation of Graphite into Graphene. *RSC Adv.* **2017**, *7*, 52252–52260, doi:10.1039/c7ra07489a.
59. Nguyen, A.T.; Lee, Y.; Nguyen, P.Q.H.; Dera, P.; Yoon, S.H.; Lee, W. Enhancing the Electrical Properties of Graphite Nanoflake through Gamma-Ray Irradiation. *Sci. Rep.* **2022**, *12*, 1–7, doi:10.1038/s41598-022-19232-2.
60. Sharmila, D.A.S.; Rathuwadu, N.P.W. The Effect of Nitrogen-Based Additives on the Synthesis of Modified Graphene Materials and Their Performance in Supercapacitor Applications. *Discov. Appl. Sci.* **2025**, *7*, 1196, doi:10.1007/s42452-025-07729-0.
61. Yang, W.; Zhou, J.; Wang, S.; Wang, Z.; Lv, F.; Zhang, W.; Zhang, W.; Sun, Q.; Guo, S. A Three-Dimensional Carbon Framework Constructed by N/S Co-Doped Graphene Nanosheets with Expanded Interlayer Spacing Facilitates Potassium Ion Storage. *ACS Energy Lett.* **2020**, *5*, 1653–1661, doi:10.1021/acsenergylett.0c00413.
62. Liang, S.; Mu, L.; Chen, L.; Jiang, J.; Yang, Y.; Fang, H. Tuning the Interlayer Spacings in Dry Graphene Oxide Membranes via Ions. *Chem.—An Asian J.* **2020**, *15*, 2346–2349, doi:10.1002/asia.202000251.
63. He, T.; Meng, X.; Nie, J.; Tong, Y.; Cai, K. Thermally Reduced Graphene Oxide Electrochemically Activated by Bis-Spiro Quaternary Alkyl Ammonium for Capacitors. *ACS Appl. Mater. Interfaces* **2016**, *8*, 13865–13870, doi:10.1021/acsami.6b00885.
64. Sharma, P.; Sharma, G.; Punia, R. Synthesis of Graphene from Activated Carbon at Liquid Nitrogen Temperature and Its Detailed Structural Analysis. *Appl. Phys. A Mater. Sci. Process.* **2021**, *127*, 1–7, doi:10.1007/s00339-021-04416-w.
65. Sieradzka, M.; Ślusarczyk, C.; Fryczkowski, R.; Janicki, J. Insight into the Effect of Graphite Grain Sizes on the Morphology, Structure and Electrical Properties of Reduced Graphene Oxide. *J. Mater. Res. Technol.* **2020**, *9*, 7059–7067, doi:10.1016/j.jmrt.2020.05.026.
66. Perrotta, M.L.; Macedonio, F.; Tocci, E.; Giorno, L.; Drioli, E.; Gugliuzza, A. Graphene Stimulates the Nucleation and Growth Rate of Nacl Crystals from Hypersaline Solution via Membrane Crystallization†. *Environ. Sci. Water Res. Technol.* **2020**, *6*, 1723–1736, doi:10.1039/c9ew01124b.
67. Love-baker, C.A.; Harrell, T.M.; Vautard, F.; Klett, J.; Li, X. Analysis of the Turbostratic Structures in PAN-Based Carbon Fibers with Wide-Angle x-Ray Diffraction. *Carbon N. Y.* **2024**, *224*, 119037, doi:10.1016/j.carbon.2024.119037.
68. Dočkal, J.; Moučka, F.; Lísal, M. Molecular Dynamics of Graphene-Electrolyte Interface: Interfacial Solution Structure and Molecular Diffusion. *J. Phys. Chem. C* **2019**, *123*, 26379–26396, doi:10.1021/acs.jpcc.9b07487.
69. Pykal, M.; Langer, M.; Blahová Prudilová, B.; Banáš, P.; Otyepka, M. Ion Interactions across Graphene in Electrolyte Aqueous Solutions. *J. Phys. Chem. C* **2019**, *123*, 9799–9806, doi:10.1021/acs.jpcc.8b12055.

 doi:10.20944/preprints202606.0364.v1

70. De Rosa, S.; Branchini, P.; Yivlialin, R.; Duò, L.; Bussetti, G.; Tortora, L. Disclosing the Graphite Surface Chemistry in Acid Solutions for Anion Intercalation. *ACS Appl. Nano Mater.* **2020**, *3*, 691–698, doi:10.1021/acsanm.9b02220.
71. Song, Y.; Yang, H.; Wang, Y.; Chen, S.; Li, D.; Zhang, S.; Zhang, X. Controlling the Assembly of Graphene Oxide by an Electrolyte-Assisted Approach. *Nanoscale* **2013**, *5*, 6458–6463, doi:10.1039/c3nr01188g.
72. Bandas, C.; Popescu, M.I.; Orha, C.; Nicolaescu, M.; Pop, A.; Lazau, C. Development of Hybrid Electrodes Based on a Ti/TiO2 Mesoporous/Reduced Graphene Oxide Structure for Enhanced Electrochemical Applications. *Coatings* **2023**, *13*, 1359, doi:10.3390/coatings13081359.
73. Singh, K.; Khanna, V.; Chaudhary, V.; Jasrotia, R.; Prakash, C.; Al-Kahtani, A.A. Investigating the Potential of Powder Metallurgy for Fabricating Graphene Nanoplatelets Reinforced Copper Nanocomposites. *J. Mater. Res. Technol.* **2024**, *31*, 1258–1269, doi:10.1016/j.jmrt.2024.06.138.
74. Aldalbahi, A.; Rahaman, M.; Almoiqli, M. Performance Enhancement of Modified 3D SWCNT/RVC Electrodes Using Microwave-Irradiated Graphene Oxide. *Nanoscale Res. Lett.* **2019**, *14*, 351, doi:10.1186/s11671-019-3174-9.
75. James, A.; Rahman, M.R.; Mohamad Said, K.A. bin; Namakka, M.; Shahabuddin, M.; Al-Saleem, M.S.M.; Al-Humaidi, J.Y.; Rahman, M.M.; Salam, M.A. Multifunctional PVDF Membranes Incorporating Graphene, TiO2, and Nanocellulose: Synergistic Effects on Filtration and Antifouling Performance. *RSC Adv.* **2025**, *15*, 31471–31497, doi:10.1039/d5ra04672f.
76. Ghosh, M.; Ray, A.; Rao, G.M. Performance Dependence of Electrochemical Capacitor on Surface Morphology for Vertically Aligned Graphene Nanosheets. *Ionics (Kiel).* **2020**, *26*, 981–990, doi:10.1007/s11581-019-03254-4.
77. Ferrer, P.R.; Mace, A.; Thomas, S.N.; Jeon, J.W. Nanostructured Porous Graphene and Its Composites for Energy Storage Applications. *Nano Converg.* **2017**, *4*, 29, doi:10.1186/s40580-017-0123-0.
78. Rahman, S. ur; Ahmed, W.; Rehman, N.U.; Alkhedher, M.; Tag El Din, E.S.M. Fabrication of Graphene Sheets Using an Atmospheric Pressure Thermal Plasma Jet System. *Energies* **2022**, *15*, 7245, doi:10.3390/en15197245.
79. Ali, A.; Liang, F.; Zhu, J.; Shen, P. The Role of Graphene in Rechargeable Lithium Batteries: Synthesis, Functionalisation, and Perspectives. *Nano Mater. Sci.* **2025**, *7*, 818–836, doi:10.1016/j.nanoms.2022.07.004.
80. Thangaraj, B.; Mumtaz, F.; Abbas, Y.; Anjum, D.H.; Solomon, P.R.; Hassan, J. Synthesis of Graphene Oxide from Sugarcane Dry Leaves by Two-Stage Pyrolysis. *Molecules* **2023**, *28*, doi:https://doi.org/10.3390/molecules28083329.
81. Zhang, M.; Li, P.; Wu, D. Editorial for Special Issue: "Synthesis and Application of Biomass-Derived Carbon-Based Nanomaterial." *Nanomaterials* **2023**, *13*, 2020, doi:10.3390/nano13132020.
82. Mehmandoust, M.; Li, G.; Erk, N. Biomass-Derived Carbon Materials as an Emerging Platform for Advanced Electrochemical Sensors: Recent Advances and Future Perspectives. *Ind. Eng. Chem. Res.* **2023**, *62*, 4628–4635, doi:10.1021/acs.iecr.2c03058.
83. Anagbonu, P.; Ghali, M.; Allam, A. Low-Temperature Green Synthesis of Few-Layered Graphene Sheets from Pomegranate Peels for Supercapacitor Applications. *Sci. Rep.* **2023**, *13*, 1–12, doi:10.1038/s41598-023-42029-w.
84. Liu, T.; Liu, Y.; Liu, M.; Wang, Y.; He, W.; Shi, G.; Hu, X.; Zhan, R.; Luo, G.; Xing, M.; et al. Synthesis of Graphene Oxide-Quaternary Ammonium Nanocomposite with Synergistic Antibacterial Activity to Promote Infected Wound Healing. *Burn. Trauma* **2018**, *6*, 1–23, doi:10.1186/s41038-018-0115-2.
85. Chen, Y.; Shi, L.; Yuan, Q.; Li, A.; Huang, S.; Yang, H.Y.; Chen, X.; Zhou, J.; Song, H. Crystallization-Induced Morphological Tuning Toward Denim-like Graphene Nanosheets in a KCl-Copolymer Solution. *ACS Nano* **2018**, *12*, 4019–4024, doi:10.1021/acsnano.8b01708.
86. Wang, Y.; Song, Y.; Watanabe, S.; Zhang, S.; Li, D.; Zhang, X. Stitching Chemically Converted Graphene on Solid Surfaces by Solvent Evaporation. *ACS Appl. Mater. Interfaces* **2012**, *4*, 6443–6449, doi:10.1021/am302225y.
87. Mokhtarifar, M.; Arab, H.; Maghrebi, M.; Baniadam, M. Amine-Functionalization of Carbon Nanotubes Assisted by Electrochemical Generation of Chlorine. *Appl. Phys. A Mater. Sci. Process.* **2018**, *124*, 0, doi:10.1007/s00339-017-1438-8.

 doi:10.20944/preprints202606.0364.v1

88. Navalon, S.; Dhakshinamoorthy, A.; Alvaro, M.; Antonietti, M.; García, H. Active Sites on Graphene-Based Materials as Metal-Free Catalysts. *Chem. Soc. Rev.* **2017**, *46*, 4501–4529, doi:10.1039/c7cs00156h.
89. Sun, D.; Tan, Z.; Tian, X.; Ke, F.; Wu, Y.; Zhang, J. Graphene: A Promising Candidate for Charge Regulation in High-Performance Lithium-Ion Batteries. *Nano Res.* **2021**, *14*, 4370–4385, doi:10.1007/s12274-021-3405-0.
90. Lizée, M.; Esfandiar, A.; Panoni, E.; Mischenko, A.; Taberna, P.L.; Simon, P.; Bocquet, L. Disentangling Conduction Pathways at the Ionic–Electronic Interface in EMI-TFSI-Covered Graphene Transistors. *Proc. Natl. Acad. Sci. U. S. A.* **2025**, *122*, 1–6, doi:10.1073/pnas.2426506122.
91. Tarigan, K.; Siburian, R.; Sitorus, E.A.M.; Purba, F.J.; Manik, Y.G.O. Fabrication and Optimization of Primary Batteries Using Ni/Graphene Nanosheet Electrodes. *Sci. Technol. Indones.* **2024**, *9*, 413–426, doi:10.26554/sti.2024.9.2.413-426.
92. Abbas, G.; Sonia, F.J.; Jindra, M.; Červenka, J.; Kalbáč, M.; Frank, O.; Velický, M. Electrostatic Gating of Monolayer Graphene by Concentrated Aqueous Electrolytes. *J. Phys. Chem. Lett.* **2023**, *14*, 4281–4288, doi:10.1021/acs.jpclett.3c00814.
93. Xu, K.; Lu, H.; Kinder, E.W.; Seabaugh, A.; Fullerton-Shirey, S.K. Monolayer Solid-State Electrolyte for Electric Double Layer Gating of Graphene Field-Effect Transistors. *ACS Nano* **2017**, *11*, 5453–5464, doi:10.1021/acsnano.6b08505.
94. Liu, G.; Li, X.; Li, C.; Zheng, Q.; Wang, Y.; Xiao, R.; Huang, F.; Tian, H.; Wang, C.; Chen, X.; et al. Efficient Fabrication of Disordered Graphene with Improved Ion Accessibility, Ion Conductivity, and Density for High-Performance Compact Capacitive Energy Storage. *Adv. Sci.* **2024**, *11*, 1–12, doi:10.1002/advs.202405155.
95. Rani, J.R.; Thangavel, R.; Kim, M.; Lee, Y.S.; Jang, J.H. Ultra-High Energy Density Hybrid Supercapacitors Using Mno2/Reduced Graphene Oxide Hybrid Nanoscrolls. *Nanomaterials* **2020**, *10*, 2049, doi:10.3390/nano10102049.
96. Obeidat, A.M.; Luthra, V.; Rastogi, A.C. Solid-State Graphene-Based Supercapacitor with High-Density Energy Storage Using Ionic Liquid Gel Electrolyte: Electrochemical Properties and Performance in Storing Solar Electricity. *J. Solid State Electrochem.* **2019**, *23*, 1667–1683, doi:10.1007/s10008-019-04272-y.
97. Zhan, C.; Liu, W.; Hu, M.; Liang, Q.; Yu, X.; Shen, Y.; Lv, R.; Kang, F.; Huang, Z.H. High-Performance Sodium-Ion Hybrid Capacitors Based on an Interlayer-Expanded MoS2/RGO Composite: Surpassing the Performance of Lithium-Ion Capacitors in a Uniform System. *NPG Asia Mater.* **2018**, *10*, 775–787, doi:10.1038/s41427-018-0073-y.
98. Sasi, S.; Murali, A.; Nair, S. V.; Nair, A.S.; Subramanian, K.R.V. The Effect of Graphene on the Performance of an Electrochemical Flow Capacitor. *J. Mater. Chem. A* **2015**, *3*, 2717–2725, doi:10.1039/c4ta05785f.
99. Thareja, S.; Kumar, A. "water-In-Salt" Electrolyte-Based High-Voltage (2.7 V) Sustainable Symmetric Supercapacitor with Superb Electrochemical Performance—An Analysis of the Role of Electrolytic Ions in Extending the Cell Voltage. *ACS Sustain. Chem. Eng.* **2021**, *9*, 2338–2347, doi:10.1021/acssuschemeng.0c08604.
100. Down, M.P.; Banks, C.E. Freestanding Three-Dimensional Graphene Macroporous Supercapacitor. *ACS Appl. Energy Mater.* **2018**, *1*, 891–899, doi:10.1021/acsaem.7b00338.
101. Tatlisu, A.; Huang, Z.; Chen, R. High-Voltage and Low-Temperature Aqueous Supercapacitor Enabled by "Water-in-Imidazolium Chloride" Electrolytes. *ChemSusChem* **2018**, *11*, 3899–3904, doi:10.1002/cssc.201802046.
102. Madani, S.; Falamaki, C.; Alimadadi, H.; Aboutalebi, S.H. Binder-Free Reduced Graphene Oxide 3D Structures Based on Ultra Large Graphene Oxide Sheets: High Performance Green Micro-Supercapacitor Using NaCl Electrolyte. *J. Energy Storage* **2019**, *21*, 310–320, doi:10.1016/j.est.2018.12.003.